[5] G. A. Landrum, R. Dronskowski, *Angew. Chem.* **1999**, *111*, 1482; *Angew. Chem. Int. Ed.* **1999**, *38*, 1390.

[6] G. A. Landrum, R. Dronskowski, *Angew. Chem.* **2000**, *112*, 1598; *Angew. Chem. Int. Ed.* **2000**, *39*, 1560.

[7] Some aspects of the scenario upon onset of magnetism (antibonding character of degenerate highest crystal orbital, symmetry lowering of the underlying wavefunction upon spin polarization) resemble the classic Jahn–Teller case; however, since only electronic coordinates are involved, the term "electronic" Jahn–Teller instability is probably more appropriate.

[8] A. Decker, G. A. Landrum, R. Dronskowski, *Z. Anorg. Allg. Chem.* **2002**, *628*, 303.

[9] In fact, the change in slope of the COHP is similar to what is observed in the classical Peierls distortion of a 1D chain of H atoms. In the present case, however, only electronic coordinates are involved such that the (admittedly questionable) term "electronic" Peierls instability is better suited.

[10] E. A. Nagelschmitz, W. Jung, R. Feiten, P. Müller, H. Lueken, *Z. Anorg. Allg. Chem.* **2001**, *627*, 523.

[11] A perceptive reviewer raised the question whether an alternative *structural* distortion to a nonmagnetic form might also be possible; indeed, such "conventional" distortion could be expected to equally reduce or remove the antibonding M–M states. Nonetheless, we believe that the purely *electronic* distortion through spin polarization is the preferred choice for the ferromagnetic transition metals and their alloys since it is evidently connected with a smaller energetic penalty. If the latter becomes too large, for example, during the attempted electronic enrichment of $Sc_2FeRh_5B_2$ with even stronger antibonding Fe–Fe interactions (see text), the alternative structural distortion takes over.

[12] $Sc_2MnRu_2Rh_3B_2$ lattice parameters from Guinier measurements: $a = 9.3909(5)$ Å, $c = 3.0170(3)$ Å; the structure has also been confirmed from single-crystal data.

[13] $Sc_2FeRu_3Rh_2B_2$ lattice parameters from Guinier measurements: $a = 9.3319(9)$ Å, $c = 3.0101(5)$ Å; a corroborating refinement from single-crystal data has also been performed. There are small traces of an additional phase (probably Ru_4Fe) present in the powdery material; Ru_4Fe has been observed by D. V. Sokol'skii, L. M. Kurashvili, A. F. Burtsev, K. K. Kuzembaev, *Russ. J. Phys. Chem.* **1987**, *61*, 293.

[14] O. K. Andersen, *Phys. Rev. B* **1975**, *12*, 3060; O. K. Andersen, O. Jepsen, *Phys. Rev. Lett.* **1984**, *53*, 2571; "Tight-Binding Approach to Computational Materials Science": O. K. Andersen, C. Arcangeli, R. W. Tank, T. Saha-Dasgupta, G. Krier, O. Jepsen, I. Dasgupta, *Mater. Res. Soc. Symp. Proc.* **1998**, *491*, 3.

[15] U. von Barth, L. Hedin, *J. Phys. C* **1972**, *5*, 1629.

[16] G. Krier, O. Jepsen, A. Burkhardt, O. K. Andersen, The TB-LMTO-ASA program, version 4.7.

[17] R. Dronskowski, P. E. Blöchl, *J. Phys. Chem.* **1993**, *97*, 8617; see also website http://www.cohp.de

[18] T. Hughbanks, R. Hoffmann, *J. Am. Chem. Soc.* **1983**, *105*, 3528.

Catalytic Activity and Poisoning of Specific Sites on Supported Metal Nanoparticles**

Swetlana Schauermann, Jens Hoffmann,
Viktor Johánek, Jens Hartmann, Jörg Libuda,* and
Hans-Joachim Freund

Typically, heterogeneous catalysts are based on nanometer-sized active particles, dispersed on an inert support material. In many cases it is assumed that the unique reactivities of such surfaces arise from the simultaneous presence of different active sites. On a molecular level, however, knowledge of the reaction kinetics of such systems is scarce (see e.g. refs. [1, 2] and references therein).

Herein, we present first direct evidence for the different activity of coexisting sites on a well-defined supported-nanoparticle system. As a model reaction we choose the decomposition of methanol on well-ordered Pd crystallites. For this reaction system two competing decomposition pathways exist (Figure 1): whereas dehydrogenation to CO represents the dominating reaction channel,[3, 4] slow carbon–oxygen-bond breakage leads to formation of adsorbed carbon and CH_x species.[4–6] With increasing carbon coverage the rate of carbon–oxygen-bond breakage drops rapidly, whereas the kinetics of dehydrogenation is hardly affected. We show that on ordered Pd crystallites these carbon and hydrocarbon species preferentially block defect sites on the particles such as particle edges and steps (see Figure 1). From this, we conclude that activity for carbon–oxygen-bond breakage is

$$CH_3OH \begin{cases} \xrightarrow[\text{fast}]{-H_{2,g}} CO_{ads} \longrightarrow CO_g \\ \xrightarrow[\text{slow}]{-H_{2,g},\ -CO_{2,g},\ -H_2O_g} C_{ads} + CH_{x,ads} \end{cases}$$

Figure 1. Schematic representation of the supported Pd nanoparticles and the blocking of defect sites by carbon species during methanol decomposition.

---

[*] Dr. J. Libuda, Dipl.-Chem. S. Schauermann, Dipl.-Phys. J. Hoffmann,
Dr. V. Johánek, Dipl.-Ing. J. Hartmann, Prof. Dr. H.-J. Freund
Fritz-Haber-Institut der Max-Planck-Gesellschaft
Faradayweg 4–6
14195 Berlin (Germany)
Fax: (+49) 30-8413-4309
E-mail: libuda@fhi-berlin.mpg.de

[**] We acknowledge support of this project by the Max-Planck Society and the Deutsche Forschungsgemeinschaft through the Priority Program 1091.

drastically enhanced at the particle defect sites, whereas this is not the case for the dehydrogenation pathway. This type of detailed investigation is made possible by two factors:

1) We employed a supported model catalyst, which, in contrast to real catalysts, is characterized by a lower and controllable level of complexity and which is suitable for the application of most surface-science experimental techniques (see refs. [1, 2, 7, 8] and references therein). The model surface used is based on a well-ordered Al_2O_3 film on a NiAl(110) single crystal.[9] On this model support, Pd particles are grown under well-controlled conditions in ultra-high vacuum (UHV). The geometric and electronic structure as well as the adsorption properties of these particles have been characterized extensively.[10–14] Briefly, the Pd aggregates represent well-shaped crystallites with an average size of approximately 6 nm. They grow in the (111) orientation and predominantly expose (111) facets as well as a small fraction of (100) facets. In Figure 2a a scanning tunneling microscopy (STM) image of the Pd particles is shown and a schematic model is displayed in Figure 1. Further structural details can be found in the literature.[13]

2) Kinetic measurements were made on these model surfaces by using molecular-beam techniques (e.g. refs. [2, 15, 16]) which provide a unique way to derive detailed kinetic information, for example, by enabling us to modulate reactant fluxes in a flexible way, determine exact reaction probabilities, or detect reaction products in a collision-free manner. To perform such experiments on supported model catalysts, we used a molecular-beam system which allows up to three beams to cross on the sample surface and perform time-resolved reflection–absorption IR spectroscopy (TR-RAIRS) and angle resolved/integrated gas–phase detection, simultaneously.[17] Recently, we have applied the molecular-beam approach to the CO oxidation on supported model catalysts.[18, 19] Here, we focus on the methanol decomposition as a first example of a more complex reaction system.

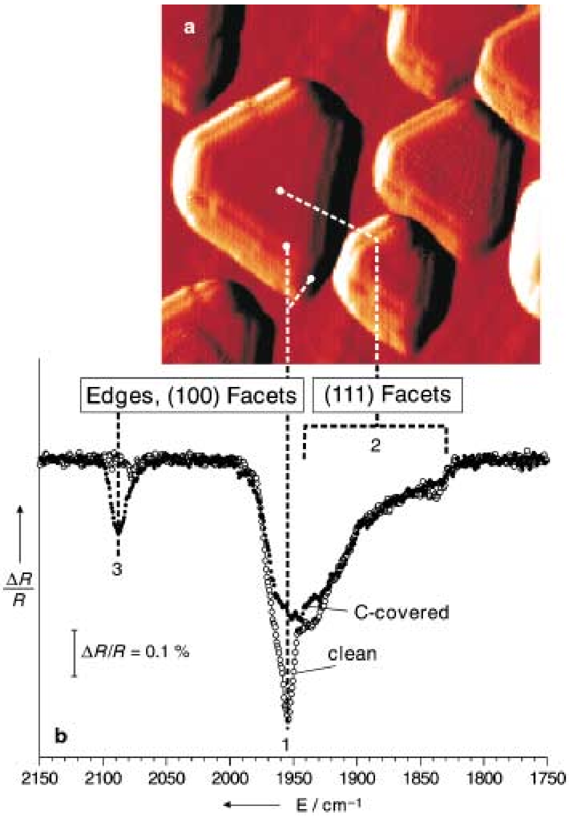

Figure 2. a) STM image of the Pd particles grown at 300 K on Al_2O_3/NiAl(110) (20 nm × 20 nm), from ref. [17]; b) RAIR spectra for CO adsorbed on $Pd/Al_2O_3/NiAl(110)$ (sample temperature 100 K, after CO exposure at 300 K); R = reflectivity open symbols: immediately after preparation; solid symbols: after prolonged exposure to methanol at 440 K.

In brief, molecular adsorption of methanol is followed by the formation of methoxy species on the Pd particles. This first intermediate is stable up to temperatures of 200 K. At higher temperatures, decomposition proceeds by two competing reaction pathways. Dehydrogenation as the dominating reaction channel results in rapid formation of CO. Depending on the rate of CO formation and desorption (i.e. the surface temperature), a significant steady-state coverage of adsorbed CO is built up, which can be monitored by in situ TR-RAIRS (IR at 440 K: $\tilde{\nu}(C{=}O) = 1900, 1840\ cm^{-1}$).

As a second pathway, we observe slow breakage of the carbon–oxygen bonds, which leads to the formation of adsorbed carbon and hydrocarbon species. This assumption is corroborated by two observations: First, weak features in the C–H-stretching-frequency region (IR: $\tilde{\nu} = 2945, 2830\ cm^{-1}$) indicate the presence of CH_x-species. Such hydrocarbon species have been shown to be stable up to 500 K.[5] Second, in a temperature programmed desorption (TPD) experiment we observe desorption of hydrocarbons ($M_r = 15$, 700 K) and recombinative desorption of CO ($M_r = 28$, 800 K), which is characteristic for the presence of atomic carbon.[20]

It is essential to note that during exposure of the catalyst to CO under identical conditions no carbon formation is observed.[18] From this we infer that the carbon deposits do not originate from CO decomposition, but from breakage of the C–O bond during the methanol dehydrogenation process.

The question arises: where on the nanoparticles are the carbon deposits located? This question is answered by RAIRS with CO as a probe molecule. The corresponding spectra for the pristine Pd particles and after prolonged exposure to methanol are compared in Figure 2b.

For the pristine sample (Figure 2b), the spectrum is dominated by a sharp absorption feature at $1960\ cm^{-1}$ (1) with a broad low-frequency shoulder (2; $1930–1840\ cm^{-1}$) and an additional weak feature at $2080\ cm^{-1}$ (3). Previously, the features between $1930\ cm^{-1}$ and $1840\ cm^{-1}$ (2) have been assigned to CO adsorbed on bridge and hollow sites predominantly on Pd(111), and the absorption peak at $2080\ cm^{-1}$ (3) to on-top CO.[11, 12] A detailed comparison with previous work shows that the prominent absorption band at $1960\ cm^{-1}$ (1) originates from a superposition of bridge-bonded CO on (100) facets and CO adsorbed at defect sites, such as particle edges or steps.[11, 12] The contribution of (100) facets, however, is expected to be small because these facets are the minor fraction and because of their tilted geometry (as a consequence of the surface selection rule, IR absorption is attenuated on small, tilted facets, e.g. ref. [21]). Following these arguments, we assume that the absorption feature at $1960\ cm^{-1}$ is dominated by CO adsorbed on defect sites, mainly on steps and particle edges (see Figure 1). Note, however, that the signals are expected to be strongly modified by dipole-coupling effects.[22] As a consequence, the relative intensities do not directly reflect the relative abundance of the corresponding sites, but the defect feature at high frequency can gain intensity at the expense of the regular absorption signal at lower frequency.

After extended exposure to methanol, drastic changes are observed in the spectrum for the adsorbed CO (Figure 2b). The defect peak at 1960 cm^{-1} (1) vanishes almost completely, whereas the absorption signal in the on-top region (3) strongly increases (2090 cm^{-1}). All other features in the spectrum, in particular the region below 1950 cm^{-1} (regular facets), remain practically unchanged. Although the dipole-coupling effects mentioned above preclude a straightforward quantification, it is apparent from these observations that adsorption at particle defect sites (i.e. steps and edges) is blocked by carbon species formed by carbon–oxygen-bond breakage. We conclude that these carbon species formed by the decomposition of methanol preferentially accumulate at defect sites.

Next the effect of carbon accumulation on the kinetics of both reaction pathways was investigated. Carbon formation results in a slowly decreasing CO absorption capacity, which allows us to follow the process in situ by TR-RAIRS. To quantify the surface fraction covered by carbon, we calibrate the integral CO absorption as a function of coverage (θ_{CO}: fraction of Pd surface sites covered by CO; note that in RAIRS there is no simple relation between coverage and absorption because of the dipole-coupling effects[21]). To do so, we combine a CO sticking-coefficient measurement and a TR-RAIRS experiment. The calibration curve is used to estimate the surface fraction covered by carbon as a function of exposure time to methanol ($\theta_C(t) = \theta_{CO}(0) - \theta_{CO}(t)$, $\theta_{CO}(0)$: initial CO coverage). It is apparent that the initial rate of carbon formation is high, but drops rapidly with increasing carbon coverage (the calculated rates of carbon formation $r_C = d(\theta_{CO}(0) - \theta_{CO}(t))/dt$ are given in Figure 3). From this observation we conclude that the carbon–oxygen-bond breakage is fast only at the defect sites, which are preferentially blocked during the reaction, but not at the regular facet sites.

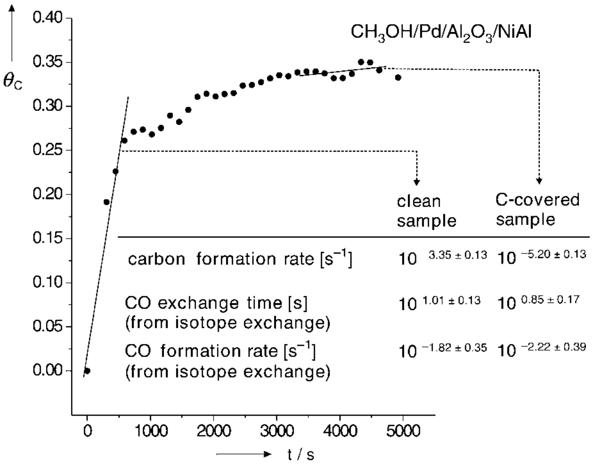

	clean sample	C-covered sample
carbon formation rate [s^{-1}]	$10^{3.35 \pm 0.13}$	$10^{-5.20 \pm 0.13}$
CO exchange time [s] (from isotope exchange)	$10^{1.01 \pm 0.13}$	$10^{0.85 \pm 0.17}$
CO formation rate [s^{-1}] (from isotope exchange)	$10^{-1.82 \pm 0.35}$	$10^{-2.22 \pm 0.39}$

Figure 3. Estimated carbon coverage as a function of exposure time *t* to the methanol beam (derived from TR-RAIRS, surface temperature of 440 K), $\theta_C = \theta_{CO}(0) - \theta_{CO}(t)$ per monolayer, and calculated rates of carbon formation (carbon–oxygen-bond breakage) and CO formation (dehydrogenation).

The next question to ask is whether the second reaction pathway, that is, the methanol dehydrogenation, is affected by carbon accumulation in a similar manner? For experimental reasons,[23] the dehydrogenation rate is determined in an isotope-exchange experiment combined with surface detection by TR-RAIRS. The setup comprises a $^{12}CH_3OH$ beam and a $^{13}CH_3OH$ beam of equal intensity. Switching between the two beams, we follow the exchange between the dehydrogenation products ^{12}CO and ^{13}CO (IR at 440 K: $\tilde{\nu}(^{12}C{=}O) = 1900, 1840\ cm^{-1}$; $\tilde{\nu}(^{13}C{=}O) = 1860, 1800\ cm^{-1}$) and determine the time constants for CO exchange τ_{CO} on the clean and the partially carbon-covered catalyst. Moreover, we can use the steady-state coverages of CO (see above) to derive the corresponding rates of CO formation (or methanol dehydrogenation) as $r_{CO} = \theta_{CO}\tau_{CO}^{-1}$ (Figure 3).

It is apparent that whereas the rate of carbon–oxygen-bond breakage drastically decreases with increasing carbon coverage, the rate constant for CO exchange remains nearly unaffected by this process. The decrease in the dehydrogenation rate simply reflects the decrease in the carbon-free Pd surface area. Quantitatively, we find that the ratio between the rates of dehydrogenation and carbon–oxygen-bond breakage r_{CO}/r_C increases from 30 on the pristine sample to approximately 1000 on the carbon-contaminated sample.

In conclusion we have presented the first direct evidence for the different activity of various reactive sites coexisting on a well defined supported metal catalyst. Combining molecular-beam methods and TR-RAIRS, we have investigated the kinetics of methanol decomposition on well-ordered Pd crystallites. Two competing reaction pathways are observed, the rapid dehydrogenation to give CO and the slow carbon–oxygen-bond breakage leading to formation of carbon and hydrocarbon species. Employing CO as a probe molecule, it is shown the carbon-oxygen bond breakage occurs preferentially at particle step and edge sites, whereas this is not the case for dehydrogenation.

Experimental Section

All experiments were performed in a UHV molecular beam apparatus at the Fritz-Haber-Institute (Berlin) which allows up to three beams to be crossed on the sample surface.[17] The CH_3OH beam (Merck, >99.8%) and the $^{13}CH_3OH$ beam (Cambridge Isotope Laboratories, >99%) are generated by effusive multichannel-array sources. For all methanol experiments the surface temperature was 440 K and the beam intensity was 5.3×10^{14} molecules$cm^{-2}s^{-1}$. The RAIR spectra in Figure 2 were recorded (at 100 K after CO saturation at 300 K) before and after exposure to a methanol dose of 2.5×10^{18} moleculescm^{-2}. The rates given in Figure 3 for the partially carbon-covered sample correspond to a similar methanol dose. For the isotope-exchange experiments, beam modulation was provided by computer-controlled shutters located inside the second pumping stages of the beam sources. For coverage calibration, CO sticking-coefficient measurements were performed using a quadrupole mass spectrometer (ABB Extrel) and a beam generated from a supersonic expansion (2.2×10^{13} molecules$cm^{-2}s^{-1}$, sample temperature 300 K). All IR spectra were acquired employing a vacuum FT-IR spectrometer (Bruker IFS 66v) at a spectral resolution of 2 cm^{-1}.

The aluminum oxide film was prepared by sputtering and annealing of a NiAl(110) single crystal, followed by an oxidation and annealing procedure, the details of which are given elsewhere.[9] Cleanliness and quality of the oxide film was checked by LEED (low-energy electron diffraction) and

AES (auger electron spectroscopy). Before the experiment, Pd (>99.9%) was deposited by evaporation from a rod by using a commercial evaporator (Focus, EFM 3) based on electron bombardment (Pd coverage: 2.7 × 10^{15} cm^{-2}, sample temperature: 300 K). The evaporator flux was calibrated by a quartz microbalance prior to use. After preparation the Pd particles were stabilized by oxygen and CO exposure as discussed previously.[13, 24]

Received: March 1, 2002 [Z18807]

[1] V. P. Zhdanov, B. Kasemo, *Surf. Sci. Rep.* **2000**, *39*, 25, and references therein.

[2] C. R. Henry, *Surf. Sci. Rep.* **1998**, *31*, 231, and references therein.

[3] G. A. Kok, A. Noordermeer, B. E. Nieuwenhuys, *Surf. Sci.* **1983**, *135*, 65.

[4] R. P. Holroyd, M. Bowker, *Surf. Sci.* **1997**, *377–379*, 786.

[5] M. Rebholz, N. Kruse, *J. Chem. Phys.* **1991**, *95*, 7745.

[6] J.-J. Chen, Z.-C. Jiang, Y. Zhou, B. R. Chakraborty, N. Winograd, *Surf. Sci.* **1995**, *328*, 248.

[7] H.-J. Freund, *Angew. Chem.* **1997**, *109*, 444; *Angew. Chem. Int. Ed. Engl.* **1997**, *36*, 452.

[8] K. Hayek, B. Jenewein, B. Klotzer, W. Reichl, *Top. Catal.* **2001**, *12*, 25, and references therein.

[9] J. Libuda, F. Winkelmann, M. Bäumer, H.-J. Freund, T. Bertrams, H. Neddermeyer, K. Müller, *Surf. Sci.* **1994**, *318*, 61.

[10] M. Bäumer, H.-J. Freund, *Prog. Surf. Sci.* **1999**, *61*, 127.

[11] K. Wolter, O. Seiferth, H. Kuhlenbeck, M. Bäumer, H.-J. Freund, *Surf. Sci.* **1998**, *399*, 190.

[12] M. Frank, M. Bäumer, *Phys. Chem. Chem. Phys.* **2000**, *2*, 4265.

[13] I. Meusel, J. Hoffmann, J. Hartmann, M. Heemeier, M. Bäumer, J. Libuda, H.-J. Freund, *Catal. Lett.* **2001**, *71*, 5.

[14] S. Shaikhutdinov, M. Frank, M. Bäumer, S. D. Jackson, R. Oldman, J. C. Hemminger, H.-J. Freund, *Catal. Lett.* in press.

[15] M. P. D'Evelyn, R. J. Madix, *Surf. Sci. Rep.* **1984**, *3*, 413.

[16] M. Asscher, G. A. Somorjai in *Atomic and Molecular Beam Methods, Vol. 2* (Ed.: G. Scoles), Oxford University Press, Oxford, **1988**, p. 489.

[17] J. Libuda, I. Meusel, J. Hartmann, H.-J. Freund, *Rev. Sci. Instrum.* **2000**, *71*, 4395.

[18] J. Libuda, I. Meusel, J. Hoffmann, J. Hartmann, L. Piccolo, C. R. Henry, H.-J. Freund, *J. Chem. Phys.* **2001**, *114*, 4669.

[19] I. Meusel, J. Hoffmann, J. Hartmann, J. Libuda, H.-J. Freund, *J. Phys. Chem. B* **2001**, *105*, 3567.

[20] V. Matolin, M. Rebholz, N. Kruse, *Surf. Sci.* **1991**, *245*, 233.

[21] F. M. Hoffmann, *Surf. Sci. Rep.* **1983**, *3*, 107.

[22] P. Hollins, *Surf. Sci. Rep.* **1992**, *16*, 51.

[23] The fragmentation pattern of CH_3OH which like CO contains *m/z* 28 as a main fragment and the low reaction probabilities prevent rate measurements by quadrupole mass spectrometry.

[24] S. Shaikhutdinov, M. Heemeier, J. Hoffmann, I. Meusel, B. Richter, M. Bäumer, H. Kuhlenbeck, J. Libuda, H.-J. Freund, R. Oldman, S. D. Jackson, C. Konvicka, M. Schmid, P. Varga, *Surf. Sci.* **2002**, *501*, 270.

Enantioselective Synthesis of Propargylamines by Copper-Catalyzed Addition of Alkynes to Enamines**

Christopher Koradin, Kurt Polborn, and Paul Knochel*

Propargylamines are important as both synthetic intermediates for the preparation of polyfunctional amino derivatives and as biologically active compounds.[1] Their preparation in enantiomerically enriched form is therefore of great importance. Although several diastereo- and enantioselective syntheses have been developed,[2] until now no metal-catalyzed enantioselective synthesis of propargylamines is known.[3] We report herein a new copper(I)-catalyzed enantioselective addition of alkynes[4] to enamines. First, we examined the racemic synthesis of propargylamines by metal-complex catalysis. Various metal salts, including $Sc(OTf)_3$, $Zn(OTf)_2$, $Yb(OTf)_3$, and Cu^{I} and Cu^{II} salts,[5] were tested as catalysts. Copper(I) and copper(II) bromide proved to give the fastest conversions. We chose test enamines[6] with readily removable protecting groups such as an allyl or a benzyl group. Enamines **1a–h** (1.2–1.5 equiv) reacted readily with terminal alkynes **2a–k** in toluene in the presence of copper(I) bromide (5 mol%) to give propargylic amines of type **3** (Scheme 1, Table 1) under mild reaction conditions.

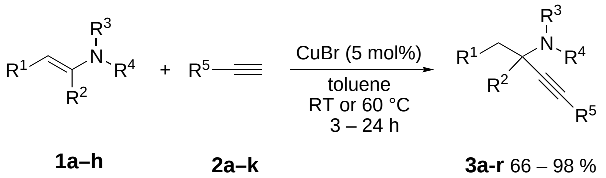

Scheme 1. Synthesis of propargylamines by the addition of alkynes to enamines.

A range of functionalized alkynes that bear a methoxy group, a double bond, a nitrile group, a chloride, a silyloxy group, an acetal, or a silyl functionality were successfully used (Table 1, entries 1–8). In the case of nitrile **2d**, the reaction required 5 h at 60 °C for complete conversion. Disubstituted enamines tend to be more reactive than trisubstituted enamines (Table 1, entries 10/15 or entries 12/17). In the case of the cyclic enamine **1h**, which is in equilibrium with a dimeric structure,[7] the reaction was carried out for 3 h at 80 °C (Table 1, entry 18).

After this study, which showed the broad scope of the reaction, we turned our attention to the enantioselective

---

[*] Prof. Dr. P. Knochel, C. Koradin, Dr. K. Polborn
Department Chemie, Ludwig-Maximilians-Universität
Butenandtstrasse 5-13, Haus F, 81377 München (Germany)
Fax: (+49) 89-2180-7680
E-mail: paul.knochel@cup.uni-muenchen.de

[**] We thank the Deutsche Forschungsgemeinschaft (Leibniz program). C.K. thanks BASF AG (Ludwigshafen) for a fellowship. We also thank Chemetall GmbH (Frankfurt) and BASF AG (Ludwigshafen) for the generous gift of chemicals.

Supporting information for this article is available on the WWW under http://www.angewandte.org or from the author.